Single and two-particle energy gaps across the disorder-driven superconductor-insulator transition

Karim Bouadim, Yen Lee Loh, Mohit Randeria, and Nandini Trivedi
Department of Physics, The Ohio State University, Columbus, OH 43210, USA

The competition between superconductivity and localization raises profound questions in condensed matter physics. In spite of decades of research, the mechanism of the superconductor-insulator transition (SIT) and the nature of the insulator are not understood. We use quantum Monte Carlo simulations that treat, on an equal footing, inhomogeneous amplitude variations and phase fluctuations, a major advance over previous theories. We gain new microscopic insights and make testable predictions for local spectroscopic probes. The energy gap in the density of states survives across the transition, but coherence peaks exist only in the superconductor. A characteristic pseudogap persists above the critical disorder and critical temperature, in contrast to conventional theories. Surprisingly, the insulator has a two-particle gap scale that vanishes at the SIT, despite a robust single-particle gap.

PACS numbers: 74.40.Kb,74.62.En,74.78.-w,74.81.-g

Attractive interactions between electrons lead to superconductivity, a spectacular example of *long range order* in physics, while disorder leads to *localization* of electronic states. One of the most fascinating examples of the interplay between the effects of interactions and disorder, is the destruction of superconductivity in thin films with increasing disorder (or decreasing thickness or increasing magnetic field), and the resulting superconductor-to-insulator transition (SIT) [1–9].

It was recognized long ago that s-wave superconductivity is remarkably robust against weak disorder [10, 11]. But strong disorder, where the SIT occurs, is very hard to treat theoretically in an interacting system. Early work on critical phenomena [12] at the SIT used bosonic models to describe fluctuations of the phase of the superconducting order parameter. A more microscopic approach, involving the fermionic degrees of freedom, leads to a highly inhomogeneous state [13–16]. Even though the disorder potential varies on an atomic scale, the superconducting pairing amplitude forms "self-organized" puddles on the scale of the coherence length and results in large suppression of the superfluid density [13, 14]. However, the inhomogeneous mean field theory by itself fails to capture the SIT, which necessarily requires inclusion of phase fluctuations.

In this paper we make a major advance by using quantum Monte Carlo (QMC) simulations of a microscopic model for an s-wave superconductor (SC) in a random potential, which treats on an equal footing the inhomogeneous variations of the pairing amplitude and thermal and quantum phase fluctuations. What is new in our paper are calculations of one-particle and two-particle spectral functions across the SIT which allows us to answer the questions about the mechanism of the transition, the evolution of the local excitation spectrum across the SIT and the nature of the resulting insulator.

Our main results are as follows:
(1) *Single-particle gap:* At $T = 0$ the gap in the single-particle density of states (DOS) survives through the SIT, so that one goes from a gapped superconductor to a gapped insulator. Although both states are highly inhomogeneous, the local density of states (LDOS) is gapped at every site.
(2) *Coherence peaks:* Coherence peaks – characteristic pile-ups in the DOS at the gap edges – are strongly correlated with superconducting order and vanish as the temperature is raised above T_c, or as the disorder is increased across the SIT.
(3) *Pseudogap:* Near the SIT, a pseudogap – a suppression in the low-energy DOS – persists well above the superconducting T_c, in marked deviation from BCS theory. A pseudogap also exists at finite temperatures in the insulating state.
(4) *Two-particle gap:* There is a characteristic energy scale $\omega_{\rm pair}$ to insert a pair in the insulator that collapses upon approaching the SIT from the insulating side. However, the two-particle spectral function does not have a hard gap since rare regions lead to a very small spectral weight at low energies.

Our results thus provide a complete description of the phases and the quantum critical region bounded by T_c in the superconductor and $\omega_{\rm pair}$ in the insulator. Furthermore, our predictions for the local tunneling density of states and the dynamical pair susceptibility as a function of temperature and disorder have the potential to guide future experiments using scanning tunneling spectroscopy (STS) [17–20] and other dynamical probes [21].

Model and methods: To model the competition between superconductivity and localization that leads to the SIT in quench-condensed films with thicknesses less than the coherence length, we take the simplest lattice Hamiltonian that has an s-wave superconducting ground state in the absence of disorder ($V = 0$) and exhibits Anderson localization when the attractive interaction is turned off ($U = 0$). This is the two-dimensional attrac-

tive Hubbard model in a random potential:

$$H = -t \sum_{\langle \mathbf{R}\mathbf{R}'\rangle\sigma} (c^\dagger_{\mathbf{R}\sigma} c_{\mathbf{R}'\sigma} + c^\dagger_{\mathbf{R}'\sigma} c_{\mathbf{R}\sigma}) - \sum_{\mathbf{R}\sigma} (\mu - V_{\mathbf{R}}) n_{\mathbf{R}\sigma} - |U| \sum_{\mathbf{R}} n_{\mathbf{R}\uparrow} n_{\mathbf{R}\downarrow}. \quad (1)$$

with lattice sites $\mathbf{R}$ and $\mathbf{R}'$, spin indices $\sigma =\uparrow$ or $\downarrow$, fermion creation and annihilation operators $c^\dagger$ and c , number operators $n_{\mathbf{R}\sigma} = c^\dagger_{\mathbf{R}\sigma} c_{\mathbf{R}\sigma}$, hopping t between neighboring sites $\langle \mathbf{R}\mathbf{R}'\rangle$, and chemical potential μ. $V_{\mathbf{R}}$ is a random potential at each site drawn from the uniform distribution on $[-V, +V]$, and $|U|$ is the on-site attraction leading to s-wave SC. We will measure all energies in units of t. At weak disorder this model has a superconducting ground state for any density $\langle n\rangle \neq 1$, whereas strong disorder ($V \gg 1$) localizes the fermions and destroys superconductivity.

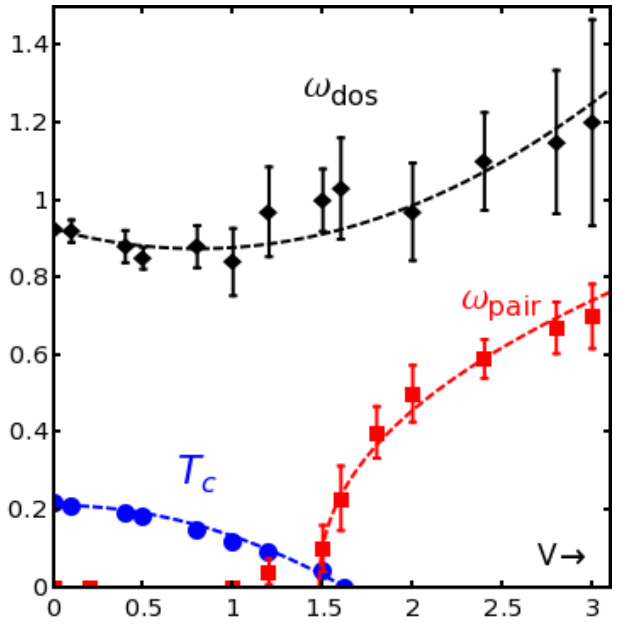

FIG. 1: **Energy and temperature scales across the superconductor-insulator transition (SIT).** The superconducting T_c (blue dots) decreases to zero at the critical disorder strength V_c. The single-particle gap $\omega_{\rm dos}$ (black diamonds), obtained from the DOS shown in Fig. 2, is large and finite in all states. The two-particle gap $\omega_{\rm pair}$ (red squares), obtained from the dynamical pair susceptibility shown in Fig. 3, is non-zero in the insulator but vanishes at the SIT. The dashed curves are guides to the eye; extracting critical exponents requires finite-size scaling beyond the scope of this paper. The statistical error bars in all the figures are dominated by disorder averaging and not from the QMC. These results were obtained at fixed attraction $|U| = 4$ and average density $\langle n\rangle \approx 0.87$ on up to 100 disorder realizations on 8×8 lattices. ω_{pair} and ω_{dos} were calculated at the lowest accessible $T = 0.1$.

We use the determinantal QMC method [22], which is free of the fermion sign problem for the Hamiltonian (1), to compute various physical observables as functions of temperature and disorder. We work at $|U| = 4$, so that the coherence length is within the system size, and work at a density $\langle n\rangle = 0.875$. We have made extensive comparisons of the QMC results with self-consistent Bogoliubov-deGennes (BdG) calculations, which only take into account only the spatial amplitude variations; see supplementary material. These comparisons permit us to separate the effects of amplitude inhomogeneity and phase fluctuations.

We compute frequency-dependent observables across the SIT for the first time. The single-particle DOS, LDOS and the pair susceptibility are obtained using the maximum entropy method (MEM) for analytic continuation [23, 24]. We have verified that these results obey various sum rules to high precision, and that the MEM correctly reproduces the low-energy structure of test spectra as shown in the supplementary material. What gives us confidence is that our central results on the single- and two-particle gaps can be equally well estimated directly from the exponential decay of the imaginary-time QMC data, without recourse to MEM.

Phase diagram: In Fig. 1 we summarize our key results for the disorder dependence of various temperature and energy scales. The Berezinskii-Kosterlitz-Thouless (BKT) critical temperature T_c is estimated from the universal jump in the superfluid density ρ_s, calculated from the transverse current correlator [25]. We note that this procedure on finite systems provide an upper bound on the actual T_c in the thermodynamic limit. As disorder strength V increases, T_c falls and finally vanishes at the critical disorder V_c, which defines the SIT. The single-particle energy gap $\omega_{\rm dos}$ remains non-zero across the SIT, whereas the two-particle energy gap $\omega_{\rm pair}$ is finite in the insulator and goes to zero at the transition. These gap scales are extracted from the DOS and the dynamical pair susceptibility, discussed below. Figure 1 can be interpreted as a phase diagram: T_c is the superconducting transition temperature, $\omega_{\rm pair}$ is a crossover scale between the insulator and the quantum critical region, and $\omega_{\rm dos}$ is the pseudogap crossover scale described below.

Single-particle spectra: We show in Fig. 2 the disorder and temperature dependence of the DOS $N(\omega)$. Panels (A,B) show the evolution with disorder at a very low temperature $T = 0.1$. The gap $\omega_{\rm dos}$ *clearly remains finite* in both superconducting and insulating states. This counterintuitive prediction agrees qualitatively with BdG theory [13, 14]. Note, however, that the coherence peaks are predominantly present in the superconducting state and absent in the insulating state. Thus, *it is the coherence peaks, and not the gap, that serve as spectral signatures of superconducting order.*

Figure 2(C,D) show the temperature evolution of $N(\omega)$ at weak disorder $V < V_c$. Unlike BCS theory, the hard SC gap does not close with increasing T. Instead, the coherence peaks gradually disappear as the temperature

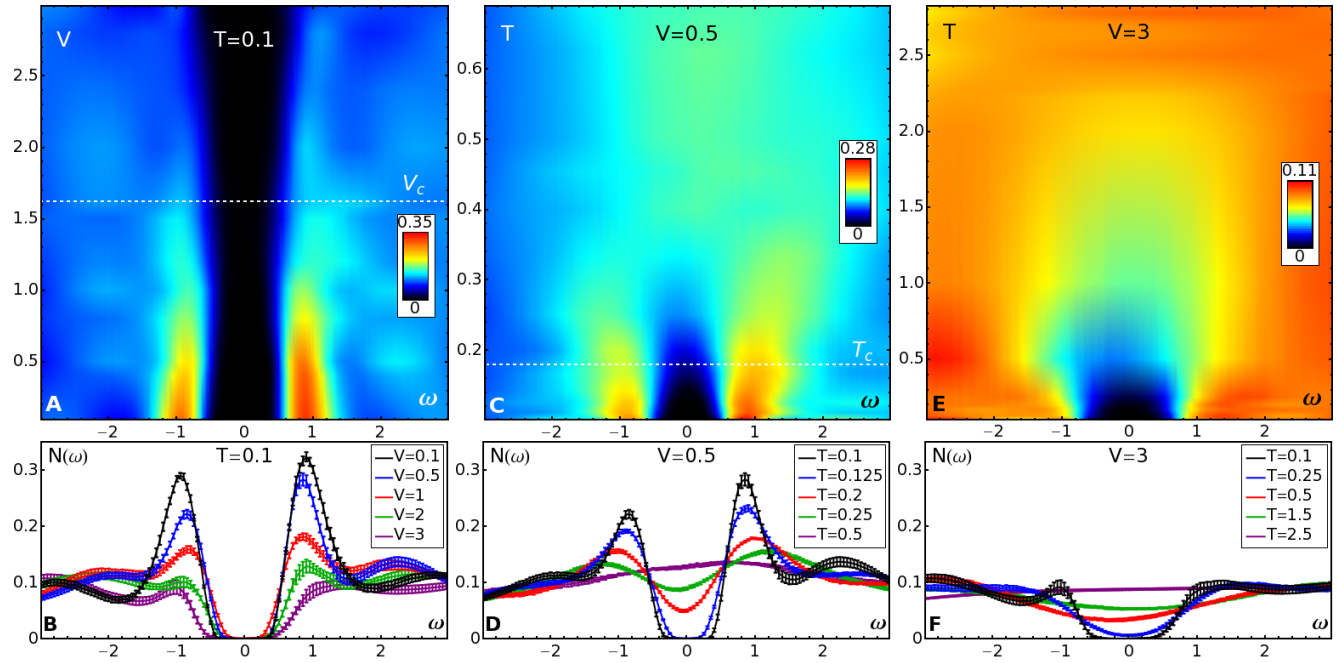

FIG. 2: **The single-particle DOS** $N(\omega)$ (upper panels) and representative spectra (lower panels), along three different cuts through the temperature-disorder plane. Panels (A,B): Disorder dependence of $N(\omega)$ at a fixed low temperature. A hard gap (black region) persists for all V above and below the SIT ($V_c \approx 1.6$), but the coherence peaks (red) exist only in the SC state and not in the insulator. Panels (C,D): T-dependence of the $N(\omega)$ for the superconductor ($V < V_c$). The coherence peaks (red) visible in the SC state, vanish for $T \gtrsim T_c \approx 0.14$. A *disorder-induced pseudogap* (loss of low-energy spectral weight) persists well above T_c. Panels (E,F): T-dependence of $N(\omega)$ for the insulator ($V > V_c$). The hard (insulating) gap at low T evolves into a pseudogap at higher T. No coherence peaks are observed at any T.

increases across T_c. Above T_c, the gap gradually fills up, with a pseudogap persisting well above T_c.

The temperature evolution of $N(\omega)$ at strong disorder $V > V_c$ is shown in Fig. 2(E,F). Here the ground state is an insulator with a hard gap and little evidence for coherence peaks, and the pseudogap persists up to an even higher temperature.

Two-particle spectra: What is the energy scale in the insulator that vanishes at the quantum critical point? We propose that it is the gap for a two-particle excitation in the insulator. To access this gap, we examine the pair susceptibility $P(\omega)$ obtained by analytical continuation of the correlation function $P(\tau) = \sum_{\mathbf{R}} \langle \mathcal{T}_\tau F(\mathbf{R};\tau) F^\dagger(\mathbf{R};0) \rangle$ where $F(\mathbf{R},\tau) = c_{\mathbf{R}\downarrow}(\tau) c_{\mathbf{R}\uparrow}(\tau)$. Thus $P(\tau)$ is the amplitude for a pair created at a site $\mathbf{R}$ at $\tau = 0$ to be found at the same site at a later time τ. We find that in the insulating phase $P(\tau)$ decays exponentially, which allows us to define ω_{pair}, the characteristic energy scale for two-particle excitations.

In Fig. 3 we show the imaginary part of the pair susceptibility $P''(\omega)$ for three disorder strengths. At weak disorder $P''(\omega)$ is very large at low ω, whereas at strong disorder it has a clear two-peak structure with a characteristic energy scale $\omega_{\rm pair}$. This dominant scale represents the typical energy required to insert a pair into the system. We find that $\omega_{\rm pair}$ collapses to zero at the SIT because there is no cost for inserting a pair into a condensate. Note that there is the possibility of low energy weight in $P"(\omega)/\omega$ originating from rare regions but their spectral weight is small.

Local probes: In Fig. 4 we track the behavior of various quantities with increasing disorder strength$V$. We show the LDOS $N(\mathbf{R},\omega)$ at representative points, maps of the spatial variation of the density $n(\mathbf{R})$, and the BdG pairing amplitude $\Delta(\mathbf{R}) = \langle c_{\mathbf{R}\downarrow} c_{\mathbf{R}\uparrow} \rangle$ (which cannot be computed in QMC). We see that the system becomes increasingly inhomogeneous with increasing disorder (moving from left to right in Fig. 4). The SIT occurs due to loss of phase coherence between superconducting islands, seen as blue patches in the pairing amplitude Δ-map.

We predict experimentally measurable signatures of the local density and pairing amplitude in the LDOS $N(\mathbf{R},\omega)$. Let us focus on three representative sites $\mathbf{R}_1$, $\mathbf{R}_2$, and $\mathbf{R}_3$. At moderate and strong disorder, $\mathbf{R}_1$ is located on a potential hill, with a low density $n(\mathbf{R}_1) \approx 0$ and a negligible pairing amplitude $\Delta(\mathbf{R}_1) \approx 0$. Thus the LDOS at $\mathbf{R}_1$ is highly asymmetric LDOS, with most of the spectral weight at $\omega > 0$, for adding an electron. In contrast, $\mathbf{R}_3$ is in a potential well, with a high density $n(\mathbf{R}_3) \approx 2$ and a negligible pairing amplitude $\Delta(\mathbf{R}_3) \approx 0$. Thus $\mathbf{R}_3$ also has a highly asymmetric LDOS, but most of the spectral weight is at $\omega < 0$, for removing an electron.

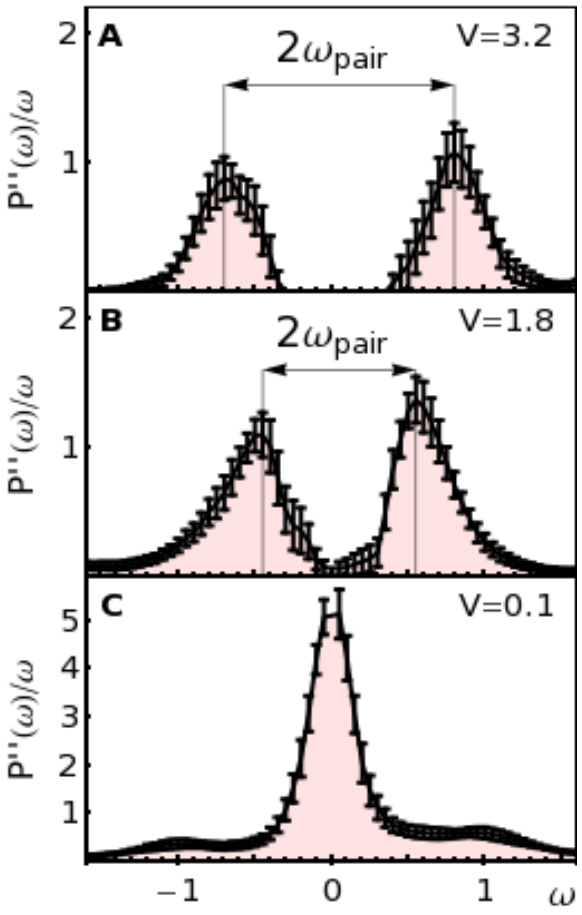

FIG. 3: **Imaginary part of the dynamical pair susceptibility** $P''(\omega)/\omega$ at $T = 0.1t$, averaged over 10 disorder realizations at three disorder strengths. Error bars represent variations between disorder realizations. For $V < V_c$, there is a large peak at $\omega = 0$, indicating zero energy cost to insert a pair into the SC. For $V > V_c$, there is a gap-like structure with an energy scale $\omega_{\rm pair}$, the typical energy required to insert a pair into the insulator which increases with V.

Finally, $\mathbf{R}_2$ lies in a superconducting puddle close to half-filling, $n(\mathbf{R}_2) \approx 1$, which permits particle mixing, and therefore a large pairing amplitude $\Delta(\mathbf{R}_2)$. The LDOS at $\mathbf{R}_2$ is much more symmetrical, with large coherence peaks that persists across the SIT and even in the insulating state. Note that all the LDOS curves have a clear gap. Thus, *the more symmetrical coherence peaks in the LDOS, and not the local energy gap, are a clear experimental signature of local pairing.*

Conclusion: A detailed picture of the superconductor to insulator transition has emerged from our microscopic calculations. Even "homogeneous disorder" arising from an uncorrelated random potential leads to a highly inhomogeneous state with superconducting puddles. These puddles shrink with increasing disorder, leading to enhanced quantum phase fluctuations that destroy phase coherence at the SIT, resulting in an unusual insulator with a large single-particle gap but a much lower energy scale for pair excitations that vanishes at the SIT. In addition, our results suggest that coherence peaks in the DOS are destroyed by thermal fluctuations for $T \gtrsim T_c$, but a pseudogap persists well above T_c. This disorder-induced pseudogap is a robust consequence of the small superfluid stiffness [26] and would exist near the SIT even in a highly disordered weak-coupling system.

Our goal was to model the disorder-driven SIT in s-wave SC films, but aspects of our results bear a striking resemblance to the completely different – and not well understood – problem of the pseudogap in underdoped cuprates. Features like the loss of low-energy spectral weight persisting across thermal or quantum phase transitions, even as coherence peaks are destroyed, may well be common to all systems where the small superfluid stiffness drives the loss of phase coherence. The cuprate pseudogap is driven by the proximity to the Mott insulator and competing order parameters, with disorder probably playing a secondary role, unlike the disorder-induced pseudogap near the SIT discussed in this paper.

We gratefully acknowledge support from grants DOE DE-FG02-07ER46423 and nsf-dmr 0706203 and computational support from Ohio Supercomputing Center.

[1] A. Goldman and N. Markovic, Physics Today **51**, 39 (1998).
[2] V. F. Gantmakher and V. T. Dolgopolov, Physics-Uspekhi **53**, 3 (2010).
[3] D. B. Haviland, Y. Liu, and A. M. Goldman, Phys. Rev. Lett. **62**, 2180 (1989).
[4] A. F. Hebard and M. A. Paalanen, Phys. Rev. Lett. **65**, 927 (1990).
[5] D. Shahar and Z. Ovadyahu, Phys. Rev. B **46**, 10917 (1992).
[6] P. W. Adams, Phys. Rev. Lett. **92**, 067003 (2004).
[7] M. A. Steiner, G. Boebinger, and A. Kapitulnik, Phys. Rev. Lett. **94**, 107008 (2005).
[8] M. D. Stewart, A. Yin, J. M. Xu, and J. M. Valles, Science **318**, 1273 (2007).
[9] S. Sachdev, *Quantum Phase Transitions* (Cambridge, London, 1999).
[10] P. W. Anderson, J. Phys. Chem. Solids **11**, 26 (1959).
[11] A. A. Abrikosov and L. P. Gorkov, Zh. Eksp. Teor. Fiz. **36**, 319 (1959).
[12] M. P. A. Fisher, G. Grinstein, and S. M. Girvin, Phys. Rev. Lett. **64**, 587 (1990).
[13] A. Ghosal, M. Randeria, and N. Trivedi, Phys. Rev. Lett. **81**, 3940 (1998).
[14] A. Ghosal, M. Randeria, and N. Trivedi, Physical ReviewB **65**, 014501 (2001).
[15] M. V. Feigel'man, L. B. Ioffe, V. E. Kravtsov, and E. A. Yuzbashyan, Phys. Rev. Lett. **98**, 027001 (2007).
[16] Y. Dubi, Y. Meir, and Y. Avishai, Nature **449**, 876 (2007), ISSN 0028-0836.
[17] B. Sacépé, C. Chapelier, T. I. Baturina, V. M. Vinokur, M. R. Baklanov, and M. Sanquer, Phys. Rev. Lett. **101**,

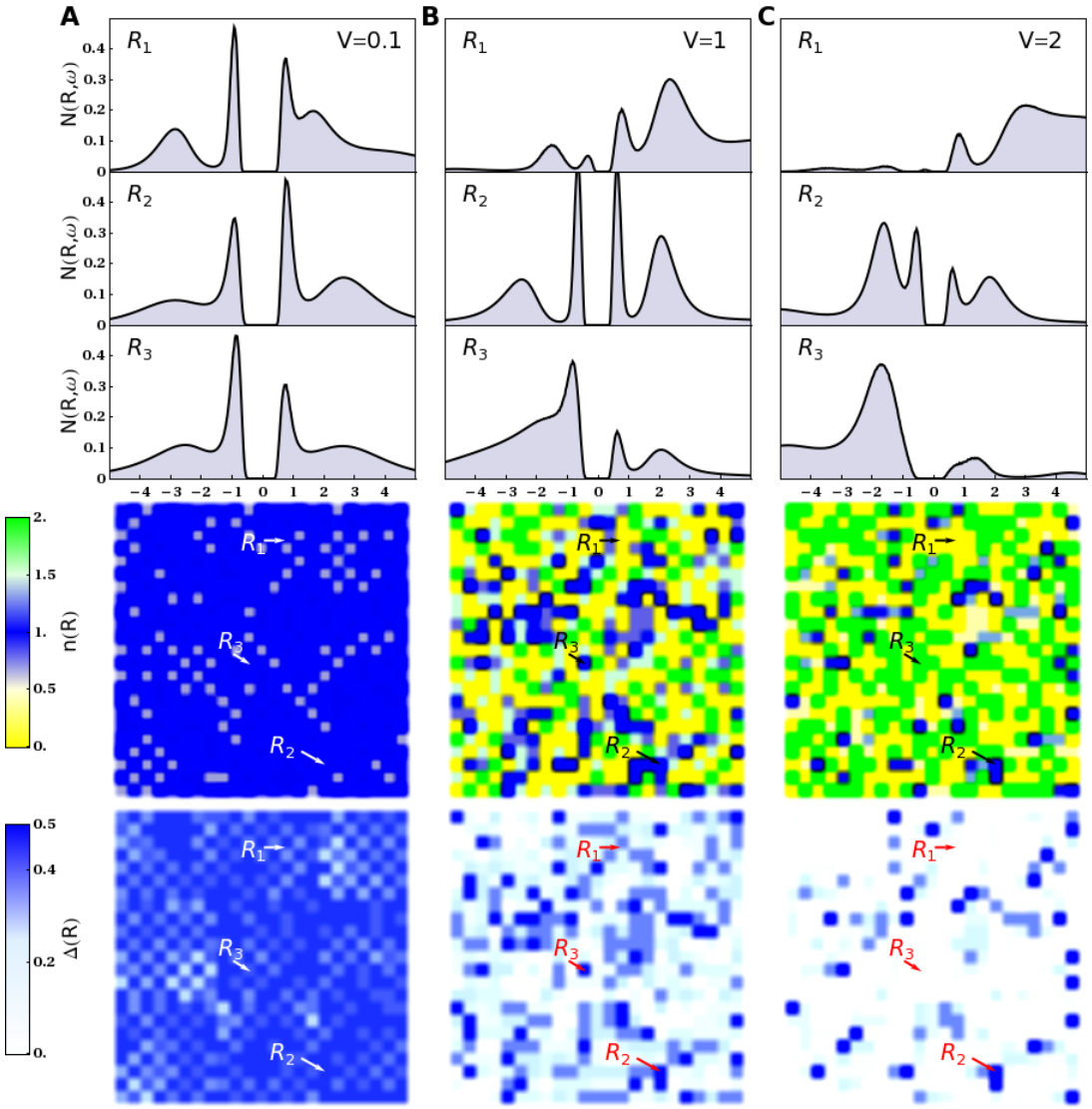

FIG. 4: Local density of states (LDOS) $N(\mathbf{R},\omega)$, density $n(\mathbf{R})$, and BdG pairing amplitude $\Delta(\mathbf{R})$ as a function of disorder strength for a montage of nine disorder realizations of 8×8 lattices. Panels A, B, C correspond to $V = 0.1, 1, 2$ respectively. The LDOS is plotted at three representative sites $\mathbf{R_i}$. At moderate and strong disorder, site $\mathbf{R_1}$ is on a high potential hill that is nearly empty, and $\mathbf{R_3}$ is in a deep valley that is almost doubly occupied. This leads to the characteristic asymmetries in the LDOS in the center and right columns for $\mathbf{R_1}$ and $\mathbf{R_3}$. The small local pairing amplitude $\Delta(\mathbf{R})$ at these two sites is reflected in the absence of coherence peaks in the LDOS. In contrast, site $\mathbf{R_2}$ has a density closer to half-filling, leading to a significant local pairing amplitude, a much more symmetrical LDOS, and coherence peaks that persist even at strong disorder.

157006 (2008).
[18] T. Cren, D. Roditchev, W. Sacks, J. Klein, J. B. Moussy, C. Deville-Cavellin, and M. Lagues, Phys. Rev. Lett. **84**, 147 (2000).
[19] K. M. Lang, V. Madhavan, E. H. J, E. W. Hudson, H. Eisaki, S. Uchida, and J. C. Davis, Nature **415**, 412 (2002).
[20] M. Vershinin, S. Misra, S. Ono, Y. Abe, Y. Ando, and A. Yazdani, Science **303**, 1995 (2004).
[21] R. W. Crane, N. P. Armitage, A. Johansson, G. Sambandamurthy, D. Shahar, and G. Grner, Phys. Rev. B **75**, 094506 (2007).
[22] R. Blankenbecler, D. J. Scalapino, and R. L. Sugar, Phys. Rev. D **24**, 2278 (1981).
[23] J. E. Gubernatis, M. Jarrell, R. N. Silver, and D. S. Sivia, Phys. Rev. B **44**, 6011 (1991).
[24] A. W. Sandvik, Phys. Rev. B **57**, 10287 (1998).
[25] D. J. Scalapino, S. R. White, and S. Zhang, Phys. Rev. B **47**, 7995 (1993).
[26] V. J. Emery and S. A. Kivelson, Nature **374**, 434 (1995).

SUPPLEMENTAL ONLINE MATERIAL

PACS numbers:

In this supplement we provide details of the determinantal QMC simulations, comparison between QMC and inhomogeneous Bogoliubov de-Gennes (BdG) mean field theory, and the analytic continuation procedure for extracting real frequency information from imaginary time QMC data.

Determinantal QMC: We use the determinantal Quantum Monte Carlo (QMC) algorithm [1, 2] to calculate the quantities discussed in the paper, including the imaginary-time Green function $G(\mathbf{R};\tau) = \left\langle \mathcal{T}_\tau c_{\mathbf{R}\sigma}(\tau) c^\dagger_{\mathbf{R}\sigma}(0) \right\rangle$ and pairing correlation function $P(\tau) = \sum_{\mathbf{R}} \left\langle \mathcal{T}_\tau F(\mathbf{R};\tau) F^\dagger(\mathbf{R};0) \right\rangle$ where $F(\mathbf{R},\tau) = c_{\mathbf{R}\downarrow}(\tau) c_{\mathbf{R}\uparrow}(\tau)$. We present results for 8×8 square lattices with periodic boundary conditions. The lattice size is dictated by the need for very accurate QMC data required for analytic continuation.

For a given set of parameters, the simulations are equilibrated for up to 4×10^5 Monte Carlo steps. The final averages for a single disorder realization are taken over 2×10^5 steps for static quantities and over 4×10^6 for dynamical quantities. We further average over 10 disorder realizations for a given disorder strength. The resulting maximum absolute errors are $\delta G(\tau) \sim 10^{-4}$ and $\delta P(\tau) \sim 10^{-2}$.

Comparisons of QMC with BdG: In Fig. 1 we show a comparison of the local density $n(\mathbf{R})$ obtained using QMC and self-consistent BdG, including inhomogeneous Hartree shifts, for one disorder pattern at different disorder strengths. The close agreement indicates that phase fluctuations, not included in BdG, have very little effect on $n(\mathbf{R})$. On the other hand, the superfluid stiffness and spectral properties at finite temperatures and large disorder are greatly affected by thermal and quantum phase fluctuations.

The local density is directly related to the occupied and unoccupied part of the LDOS (see Fig. 4 of the paper) via the sum rules: $2\int_{-\infty}^{\infty} d\omega f(\omega) N(\mathbf{R},\omega) = n(\mathbf{R})$ and $2\int_{-\infty}^{\infty} d\omega [1 - f(\omega)] N(\mathbf{R},\omega) = 1 - n(\mathbf{R})$, where $f(\omega)$ is the Fermi function and the factor of 2 comes from spin degeneracy. We have tested these sum rules for the calculated LDOS and find excellent agreement. Further sum rule tests are described below.

Analytic continuation: We use the maximum entropy method (MEM) to extract the local density of states $N(\mathbf{R},\omega)$ and the pair spectrum $P''(\omega)$ from the imaginary-time Green function $G(\mathbf{R};\tau)$ and pairing correlation function $P(\tau)$ respectively. The MEM for analytic continuation [3] essentially inverts the Laplace transforms

$$G(\mathbf{R};\tau) = \int_{-\infty}^{\infty} d\omega \frac{e^{-\tau\omega}}{1 + e^{-\beta\omega}} N(\mathbf{R},\omega), \tag{1}$$

$$P(\tau) = \int_{-\infty}^{\infty} \frac{d\omega}{\pi} \frac{e^{-\tau\omega}}{1 + e^{-\beta\omega}} P''(\omega) \coth \frac{\beta\omega}{2}. \tag{2}$$

The average DOS $N(\omega)$ is obtained from analytic continuation of $\sum_{\mathbf{R}} G(\mathbf{R},\tau)$.

We have performed extensive tests using known model spectra as follows: (i) choose a test spectrum $N(\omega)$; (ii) perform a Laplace transform to obtain the imaginary-time Green function $G(\tau)$; (iii) add random numbers $\delta G(\tau)$ drawn independently from a normal distribution of width $\delta G = 10^{-4}$, in order to simulate Monte Carlo statistical error; and finally (iv) feed the resulting noisy data, $G_{\rm data}(\tau)$, into our MEM routine. This procedure is illustrated in Fig. 2. We have concluded that the MEM is adequate for extracting the low-energy features of the spectrum, particularly the gap.

We emphasize that two of our crucial observations regarding the single particle gap scale in $N(\omega)$ and the two-particle gap scale in $P''(\omega)/\omega$ can be directly estimated, from the exponential decay at large τ of $G(\tau)$

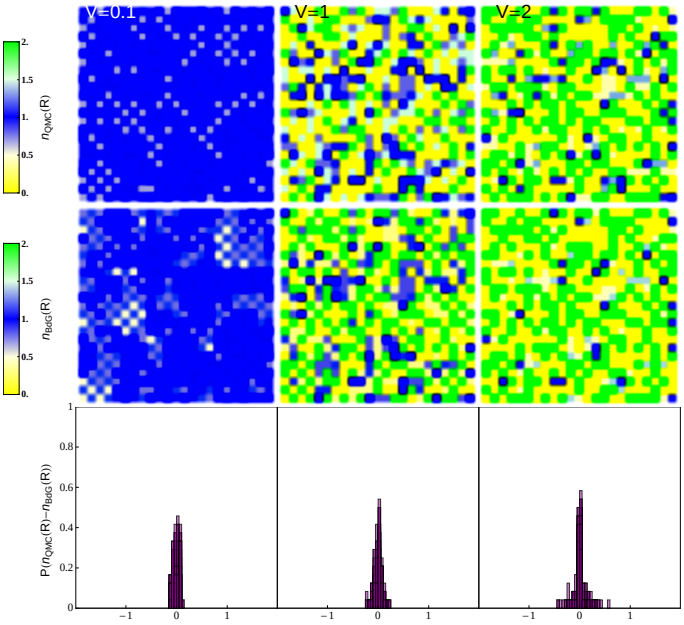

FIG. 1: Comparison of the local density $n(\mathbf{R})$ obtained using QMC (top panels) and self-consistent BdG (middle panels) for one disorder pattern at three different disorder strengths. The densities are very similar as seen from the histograms of their differences in the lowest panels, indicating that phase fluctuations have very little effect on $n(\mathbf{R})$.

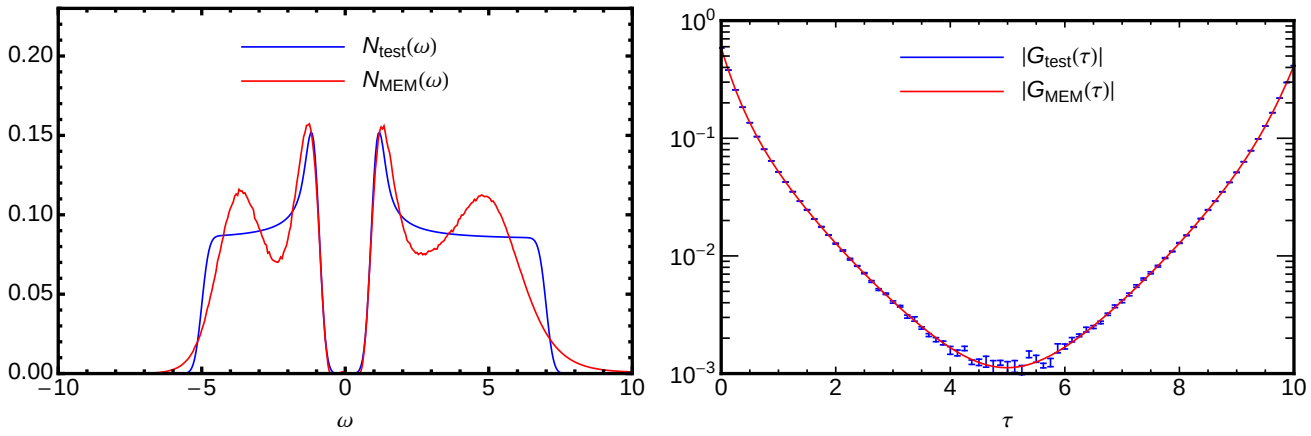

FIG. 2: Demonstration of analytic continuation using the maximum entropy method (MEM). A test spectrum (blue) is chosen, noise is added in the τ-domain, and the MEM is used to reconstruct the spectrum (red). The reconstructed Green function $G_{\text{MEM}}(\tau)$ fits the "data" $G_{\text{data}}(\tau)$ to within its error bars. The reconstructed spectrum $N_{\text{MEM}}(\omega)$ agrees well with the test spectrum $N(\omega)$ at low energies, reproducing the correct gap structure, although there are deviations at higher energies. Indeed, the magnitude of the gap can be estimated by examining the exponential decay constant of $G(\tau)$, even without using the MEM.

and $P(\tau)$ calculated from the QMC data without any MEM analytic continuation.

We have also made extensive sum-rule checks for the spectra obtained from MEM. We define $M_{\mathbf{R}}^{(m)}$, the mth frequency moment of the local density of states at position $\mathbf{R}$, as

$$M_{\mathbf{R}}^{(m)} = \int_{-\infty}^{\infty} d\omega\ \omega^m N(\mathbf{R},\omega). \tag{3}$$

These moments satisfy the following sum rules, which can be derived rigorously by extending the analysis in Ref. [4] to a disordered system:

$$M_{\mathbf{R}}^{(0)} = 1, \tag{4}$$

$$M_{\mathbf{R}}^{(1)} = V_{\mathbf{R}} - \mu + \frac{U}{2}\left\langle n_{\mathbf{R}}\right\rangle, \tag{5}$$

$$M_{\mathbf{R}}^{(2)} - M_{\mathbf{R}}^{(1)2} = zt^2 + \frac{U^2}{4}\left[2\left\langle n_{\mathbf{R}}\right\rangle - \left\langle n_{\mathbf{R}}\right\rangle^2\right], \tag{6}$$

where $z = 4$ is the coordination number. Differentiating Eq. (1) shows that the moments are also related to the values and derivatives of the Green function at $\tau = 0$ and $\tau = \beta$,

$$M_{\mathbf{R}}^{(m)} = (-1)^m\left[\frac{\partial^m G_{\mathbf{R}}}{\partial\tau^m}(0) + \frac{\partial^m G_{\mathbf{R}}}{\partial\tau^m}(\beta)\right]. \tag{7}$$

QMC simulations produce very accurate results for $G_{\mathbf{R}}(0)$ and $G_{\mathbf{R}}(\beta)$, with absolute errors of about 10^{-5}. The MEM analytic continuation procedure fits these data points to within the error bars. We have verified that the MEM LDOS satisfies the moment sum rules with a fractional error of less than 0.001% for $M^{(0)}$, less than 1% for $M^{(1)}$, and about 1% for $M^{(2)}$. In contrast, the LDOS obtained from BdG calculations are found to violate the sum rules.

[1] S. R. White, D. J. Scalapino, R. L. Sugar, E. Y. Loh, J. E. Gubernatis, and R. T. Scalettar, Phys. Rev. B **40**, 506 (1989).
[2] R. Blankenbecler, D. J. Scalapino, and R. L. Sugar, Phys. Rev. D **24**, 2278 (1981).
[3] A. W. Sandvik, Phys. Rev. B **57**, 10287 (1998).
[4] S. R. White, Phys. Rev. B **44**, 4670 (1991).